

# **Earth and Space Science**



### **RESEARCH ARTICLE**

10.1029/2024EA003697

#### **Key Points:**

- We develop and test a fully freewarebased method for estimating grain sizes of Martian dune sand and apply it to tropical dune fields
- Our grain size values fit within the envelope of grain size values from decades of previous work, indicating the validity of our method
- Our results also reveal geographic variability in grain sizes, indicating geospatial variability in sand-forming mechanisms on Mars

#### **Supporting Information:**

Supporting Information may be found in the online version of this article.

#### Correspondence to:

D. M. Burr, Devon.Burr@nau.edu

#### Citation:

Burr, D. M., Nguyen, V. N. H., Gibson, T. M.-G., & Chinchkhede, T. (2024). Estimating grain sizes of Martian dune sand: A freeware-based methodology with initial results. *Earth and Space Science*, *11*, e2024EA003697. https://doi.org/10.1029/2024EA003697

Received 19 APR 2024 Accepted 8 AUG 2024

#### **Author Contributions:**

T. Chinchkhede

Conceptualization: D. M. Burr

V. N. H. Nguyen, T. M.-G. Gibson,

Data curation: D. M. Burr,

Formal analysis: D. M. Burr
Funding acquisition: D. M. Burr
Investigation: D. M. Burr,
V. N. H. Nguyen, T. M.-G. Gibson,
T. Chinchkhede
Methodology: D. M. Burr,
V. N. H. Nguyen, T. M.-G. Gibson
Supervision: D. M. Burr
Validation: D. M. Burr
Visualization: V. N. H. Nguyen, T. M.-G. Gibson, T. Chinchkhede
Writing – original draft: D. M. Burr
Writing – review & editing: D. M. Burr

© 2024. The Author(s).

This is an open access article under the terms of the Creative Commons

Attribution License, which permits use, distribution and reproduction in any medium, provided the original work is properly cited.

# **Estimating Grain Sizes of Martian Dune Sand: A Freeware-Based Methodology With Initial Results**

D. M. Burr<sup>1</sup>, V. N. H. Nguyen<sup>2</sup>, T. M.-G. Gibson<sup>3</sup>, and T. Chinchkhede<sup>3,4</sup>

<sup>1</sup>Department of Astronomy and Planetary Science, Northern Arizona University, Flagstaff, AZ, USA, <sup>2</sup>Department of Physics and Astronomy, KU Leuven, Leuven, Belgium, <sup>3</sup>School of Earth and Atmospheric Sciences, Georgia Institute of Technology, Atlanta, GA, USA, <sup>4</sup>Department of Applied Physics and Material Science, Northern Arizona University, Flagstaff, Arizona, USA

**Abstract** Grain sizes of Martian sand dunes are critical sedimentological data on sand provenance and transport pathways. Thermal inertia values are used to characterize the grain sizes of dune sand. Most early characterizations involved single dune fields. Recent work based on global data sets has provided more widespread dune sand locations, though these data sets include the non-sandy interdune areas. To provide a more accurate grain size characterization, we leverage a global thermal inertia data set, a global dune database and a global imaging mosaic to develop a freeware-based methodology for deriving grain sizes. This methodology involves delineation of sand-only areas within dune fields and collection of thermal inertia values from those areas. We consider a unimodal histogram of values with a mode  $<\sim$  350 thermal inertia units (J m<sup>-2</sup> K<sup>-1</sup> s<sup>-1/2</sup>) to imply an effective exclusion of non-sand surfaces. Application of this methodology to dune fields for which thermal inertia values have been previous derived shows our results fall within the envelope of those values. We apply our methodology to tropical dune fields on Mars for which Dust Cover Index data imply dust-free surfaces. Conversion of these thermal inertia values to sand grain sizes yields a range of sand classifications of fine sand to granules. Comparison of sand size classifications with geographic location shows grain size ranges that are distinctive by location, consistent with local sourcing. This work points toward geographically diverse sand formation mechanisms yielding diverse grain sizes, while providing a freeware-based and thus widely accessible method for expanding the derivation of these critical data.

Plain Language Summary Knowing the sizes of sand grains on Mars provides information on the history of that sand, such as where it came from and how far it has traveled to where it is now. Sand grains of different sizes respond to heat differently, with larger sand grains heating up and cooling down more slowly than smaller grains or dust. This response to heating—termed "thermal inertia"—has been used for decades to estimate the grain sizes of dune sand on Mars. However, previous methods have been focused on only a few dune fields at a time. To increase the amount of grain size data we can collect from sand dunes on Mars, we have developed a freeware-based approach using global data sets and software that are accessible to anyone. Applying our approach to all the dunes for which grains sizes based on thermal inertia were previously derived, we show that our values are similar to those from the previous work. Applying our approach to 75 dune fields on Mars, we see different dune fields have different grain sizes, which suggests different sand formation mechanisms in these different locations. Thus, our freeware-based approach provides an accessible opportunity to learn about sand characteristics and sand histories across Mars.

#### 1. Introduction

Sand dunes have been a salient component of the Martian surface throughout its history. Analyses of both remote and in situ imaging data have revealed many geospatially disparate aeolian paleobedforms and ancient sandstone outcrops (Diniega et al., 2022). Dune fields have been shown to be changing and moving planet-wide under modern-day conditions (e.g., Bourke et al., 2008; Bridges, Bourke, et al., 2012; Chojnacki et al., 2019), demonstrating the on-going influence of aeolian sand on the Mars surface.

These contemporary dune fields have wide-spread distribution and influence (e.g., Fenton et al., 2019). The first global mapping of Mars dune fields, the Mars Global Digital Dune Database (MGD<sup>3</sup>) (Hayward et al., 2007; Hayward et al., 2014; Figure 1), was based on daytime thermal infrared (IR) data from the Thermal Emission Imaging System (THEMIS) on the Mars Odyssey spacecraft (Christensen et al., 2003, 2004), which provided near-global coverage and useful resolution (res. 100 m/px) for delineating large dune fields. Subsequent mapping

BURR ET AL. 1 of 17

23335084, 2024, 9, Downloaded from https://agupubs.onlinelibrary.wiley.com/doi/10.1029/2024E,0003697, Wiley Online Library on [29/06/2025]. See the Terms and Conditions (https://onlinelibrary.

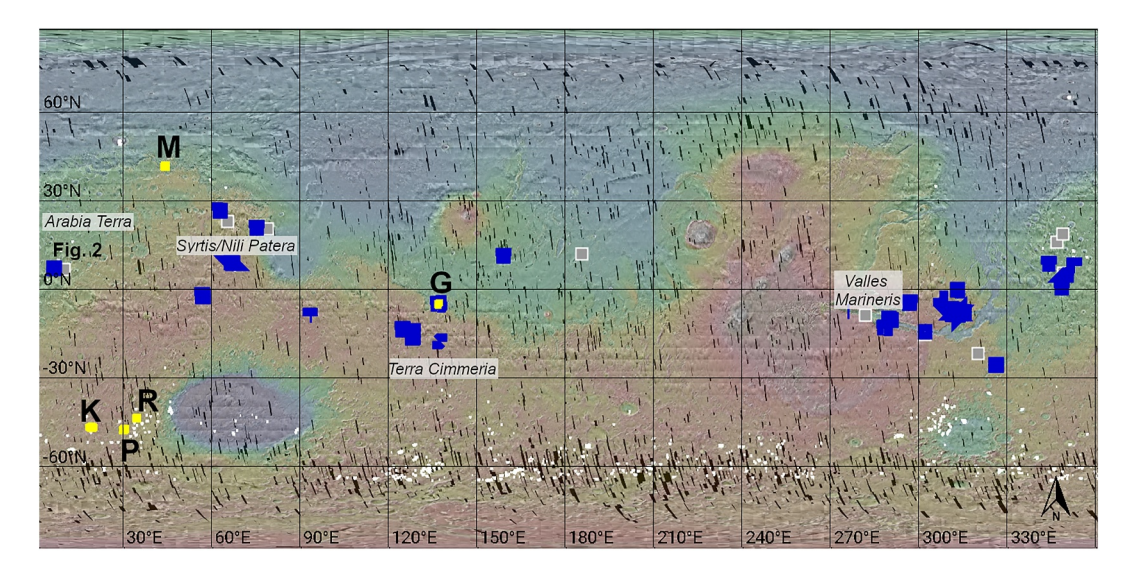


**Figure 1.** Global map of colorized elevation (warm colors are high, cool colors are low), overlain by a black-and-white mosaic of visible wavelength images (Dickson et al., 2018; darker rectangular areas are gores in the coverage of this data set), overlain by the USGS Equatorial Mars Global Digital Dune Database (MGD<sup>3</sup>; white polygons; Hayward et al., 2007). Within the tropical MGD<sup>3</sup> dune fields, delineated sandy areas with unimodal thermal inertia histograms having modal value of <~350 tiu are shown as bright blue polygons and so used in subsequent analyses. Sandy areas found to have multimodal histograms and so not used in subsequent analyses are shown as gray squares. The locations of the dune fields in Kaiser, Rabe, Proctor, Moreux, and Gale craters are shown as yellow squares with black letters. The location of Figure 2 is also indicated. Figure created using JMARS (Christensen et al., 2009). At the equator, 10° longitude equates to 590 km.

used a global mosaic (Dickson et al., 2018) of visible wavelength images from the Context Camera (CTX; res. 6 m/px; Malin & Edgett, 2001), allowing for detection and delineation of smaller dune fields (Fenton, 2020).

Along with providing daytime IR images, the THEMIS instrument also provides nighttime IR images (Christensen et al., 2003, 2004). Those THEMIS nighttime temperature data have been converted into thermal inertia values (Fergason, Christensen, & Kieffer, 2006). Thermal inertia quantifies the resistance of a material to change in temperature and is defined as  $I = (\kappa \rho c)^{1/2}$  where I is the thermal inertia (given for THEMIS data in metric thermal inertia units of J m<sup>-2</sup> K<sup>-1</sup> s<sup>-1/2</sup>, hereafter referred to as tiu),  $\kappa$  is the thermal conductivity of the material,  $\rho$  is the material density, and c is its specific heat. Given the penetration depth of the heat wave during the Martian day, thermal inertia data characterize the upper few centimeters of the Martian surface (Fergason, Christensen, & Kieffer, 2006).

Among the many uses of thermal inertia data for characterizing the surface of Mars (Mellon et al., 2008), thermal inertia data have been used to estimate grain sizes of Martian sand (Edgett & Christensen, 1991). This estimation is possible due to the disparate effects of surface materials on the components that influence thermal inertia. Whereas the density and specific heat of surface geologic materials vary by a factor of a few, the thermal conductivity at Martian surface pressures varies by an order of magnitude (Presley & Christensen, 1997a, 1997b, and references therein). For sand, the variation in thermal conductivity—and thus in thermal inertia—is in turn influenced strongly by the size of the sand grains (Edgett & Christensen, 1991). Based on this correspondence between thermal inertia and sand grain size, the presence of sand along with estimates of its grain size has been inferred (Edgett & Christensen, 1994; Putzig & Mellon, 2007) using data from the Viking Infrared Thermal Mapper (IRTM; Kieffer et al., 1977) and the Mars Global Surveyor Thermal Emission Spectrometer (TES; Christensen et al., 2001). As discussed in these references, an estimate of sand grain size from remote (orbital) data is subject to uncertainties due to the thermal effects of a mixture of sand sizes and of sand and non-sand surfaces within the map pixel of the data. However, a study that compared thermal inertia values derived from both orbital and in situ data of the Bagnold Dunes in Gale Crater found reasonable correlations between the sand grain sizes derived from remote thermal data and sand grain sizes measured in situ (Edwards et al., 2018).

Compared to other sedimentary deposits (Johnson et al., 2017), aeolian sand on Earth is commonly well-sorted (e.g., Ahlbrandt, 1979) due to the limited range of energy in the aeolian transport process. Martian sand is

BURR ET AL. 2 of 17

undergoing aeolian transport globally at terrestrial-like rates (e.g., Bourke et al., 2008; Bridges, Ayoub, et al., 2012; Bridges, Bourke, et al., 2012; Chojnacki et al., 2019; Ewing et al., 2010; Silvestro et al., 2010; Silvestro et al., 2013; Urso et al., 2018) and has been interpreted from thermal inertia data to exhibit a particularly uniform grain size compared to other surface materials (Fergason et al., 2006a, 2006b). Sand grain sizes are useful data that give insight into geologic and sedimentologic processes. As grain sizes decrease with distance of aeolian transport, mean grain size data can provide constraints on sand provenance (Ahlbrandt, 1979). Grain sizes in loose deposits like sand dune fields also offer constraints on the grain sizes of the geologic unit from which the sand is derived. In extraformational contexts, where sediment is recycled from sedimentary rocks (Cox & Lowe, 1995), grain sizes reflect and so provide evidence of this multistage provenance as has been documented from in situ data from Mars (Edgett et al., 2020). Thus, a methodology for accurate determination from remote data of sand grain sizes on Mars is highly desirable as a tool for gaining insight into the characteristics and provenance of this pervasive sand.

Because grain size has a predominant influence on thermal inertia, such that smaller grains decrease the thermal inertia whereas larger sediments or bedrock increase it, dust cover is a confounding influence on the derivation of sand grain sizes from thermal inertia data (Fergason, Christensen, & Kieffer, 2006; Mellon et al., 2008). Other factors besides the sand grain size can influence thermal inertia values derived from sediments on the Martian surface. Prior studies demonstrate that elevation (Bridges, 1994) and ice (Putzig et al., 2005) most obviously affect thermal inertia values. Examinations of the effect of mineralogy, specifically olivine, on thermal inertia did not yield consistent correlations (Brown et al., 2020; Hanna et al., 2016).

In this work, we develop, assess, and apply an open-access methodology for deriving thermal inertia values of dune sand and converting those values to sand grain sizes. We further hypothesize that in the absence of non-sand influences on thermal inertia, the derived grain sizes can be used to infer aspects of the geologic and sedimentologic processes that emplaced the sand. Application of our methodology to dune fields in the Martian tropics suggests geographically characteristic sand classifications and provide an efficient and accessible approach for a more global characterization of dune sand sizes.

#### 2. Materials and Methods

In this work, we develop a method to derive thermal inertia values from sandy areas within large dune fields and apply this methodology to a limited number of previously investigated dune fields, comparing our results with the results from those previous publications. We then apply our methodology to a broader set of tropical dune fields, specifically to more areally limited surfaces within those fields that show sandy bedforms in order to derive thermal inertia values for sand-only areas. Lastly, we analyze our results to investigate any correlations of grain sizes with geographic locations in order to detect any influence from geologic sand-production processes.

#### 2.1. Data and Technical Methods for Collecting Thermal Inertia Values of Sand

Dune fields were first mapped comprehensively on Mars between  $65^{\circ}$ N and  $65^{\circ}$ S latitude using THEMIS infrared imaging data (Hayward et al., 2007). For the 100-m resolution of the THEMIS images, the resultant data set shows moderate-to large-size dune fields (area >1 km²). Subsequent work included first an expansion of this THEMIS-based so-called "equatorial" data set to the polar regions (Hayward et al., 2014) and later a supplement of a database of smaller dune fields (mostly  $<\sim$ 5 km²) from use of the global mosaic of visible-wavelength images (Dickson et al., 2018) from the CTX.

The objective step of this work was to collect and analyze data from sandy areas. Given that dune fields have interdune areas without sand (McKee, 1979), we considered larger dune fields as more likely to provide larger contiguous sand-only areas to avoid the influence of non-sand surfaces on the data. In addition, lower latitude dune fields are more likely to avoid the influence of ice within the dunes (Fenton & Hayward, 2010; Fenton et al., 2019 and references therein), which would influence the thermal inertia (Mellon et al., 2008; Putzig et al., 2014). For these reasons, our chosen dune database for this work was the equatorial MGD<sup>3</sup> (Hayward et al., 2007).

We collected thermal inertia values from the THEMIS thermal inertia data set (Fergason, Christensen, & Kieffer, 2006). The model used to convert the THEMIS nighttime temperature data to thermal inertia values is updated from the model applied to IRTM data (Kieffer et al., 1977) and is similar to the model applied to TES data

BURR ET AL. 3 of 17

# **Earth and Space Science**

(Christensen et al., 2001), relying on a single nighttime temperature datum in combination with albedo and other inputs. Uncertainty in the output values derives from the assumption of an emission of unity and other surface material properties. Compared to previous thermal inertia models, the model applied to the THEMIS data has a more sophisticated atmospheric conceptualization and has higher spatial resolution. Compared to the resolution of the IRTM data at ~25 km/px (Chase et al., 1978) and the TES data at ~3 km/px (Christensen et al., 2001), the higher resolution of the THEMIS data is advantageous for more accurately characterizing dune field boundaries, minimizing inclusion of surrounding non-dune materials. Image-to-image variations (stripiness) in the THEMIS thermal inertia data result from seasonal atmospheric variations (Fergason, Christensen, & Kieffer, 2006) and potentially from heterogeneity in the surface thermal behavior (e.g., Putzig & Mellon, 2007).

For this work, we used THEMIS thermal inertia cubes for which the IR Calibration Flag value was 0 (images without a calibration error flag) and the Image Rating had values of 5, 6, or 7 (subjective assessment of image quality as Fair-Good, Good, Very Good, respectively; <a href="https://jmars.mars.asu.edu/">https://jmars.mars.asu.edu/</a>). For each dune field, all thermal inertia image cubes that met these criteria and coincided with the dune field polygon were loaded and data within the polygon were then collected from those cubes. This methodology was designed and accomplished within the Java Mission-planning and Analysis for Remote Sensing (JMARS) geospatial information system (Christensen et al., 2009) for maximum accessibility and is described in more detail in the Methodology Supplemental Materials accompanying this article.

#### 2.2. Compilation of Previously Derived Thermal Inertia Values for Martian Dune Fields

Thermal inertia values of dune fields have been derived from both the IRTM data set (Chase et al., 1978) and the TES data set (Christensen et al., 2001) for intracrater (in-crater) dune fields in the mid-southern and northern latitudes. In addition to these orbital characterizations of dune field thermal inertia, in situ thermal inertia values were derived for the Bagnold dune field (Edwards et al., 2018) with data from the Ground Temperature Sensor (GTS; Sébastian et al., 2010), part of the Rover Environmental Monitoring Station on the Mars Science Laboratory ("Curiosity") rover (Gómez-Elvira et al., 2012). These previously derived thermal inertia values for dune fields provide context for and comparison with our results.

#### 2.3. Collection of Thermal Inertia Data of the Sandy Surfaces

Following development and assessment of our method for deriving thermal inertia values for dune fields, we applied the method to the collection of data from sandy areas within tropical large dune fields. In sand-limited regions, dune fields may have interdune areas devoid of sand (Lancaster, 1995; McKee, 1979), and inspection shows that the MGD<sup>3</sup> polygons include areas both within and/or outside of the dune fields that are not covered by sand (Figure 2). Thus, for selected MGD<sup>3</sup> polygons, we isolated sandy areas within dune fields by delineating areas of contiguous dunes, sand sheets, or other adjacent bedforms based on appearance in the mosaic of visible-wavelength images (Dickson et al., 2018) from the CTX. Images with resolutions of a few meters to sub-meter values from the High-Resolution Imaging Science Experiment (HiRISE; McEwen et al., 1999) and the Mars Orbital Camera (MOC; Malin & Edgett, 2001) were also used where available to delineate sand boundaries. This delineation of sandy areas was initially performed on a limited number of MGD<sup>3</sup> dune field polygons by multiple mappers in order to develop experience and consistency in data collection. Subsequently, the delineation of sandy areas was divided and accomplished by individual mappers.

The dune fields used for delineation of sandy areas were selected from MGD³ polygons (Hayward et al., 2007) lying within 30° of the equator (30°N to 30°S) so as to avoid potential influences from stabilization (i.e., ice) while including a variety of geographic units and elevations. From within these delineations of sandy areas, we collected thermal inertia values from the THEMIS thermal inertia data set (Fergason, Christensen, & Kieffer, 2006) as described in Section 2.1. *Data and technical methods* above. For each delineation, a visual assessment of the type of modality for the thermal inertia values histogram and (for unimodal distributions) the modal values of those histograms were used as a check on the effectiveness of that delineation for isolating (or including) only sandy surfaces. Thermal inertia values between ~155 and ~350 tiu are indicative of sand (e.g., Fenton et al., 2003; Table 1). Because the interdune areas commonly expose non-sandy or indurated substrate (e.g., Ahlbrandt & Fryberger, 1981) having a higher thermal inertia, sand dune fields with significant interdune area, resistant knobs, or other non-sand surfaces exhibit bi- or multimodal distributions of thermal inertia histograms (Figure 2). Thus, we considered a unimodal histogram of thermal inertia values with a modal value of <~350 tiu to be indicative of

BURR ET AL. 4 of 17

2335084, 2024, 9, Downloaded from https://agupubs.onlinelibrary.wiley.com/doi/10.1029/2024E,003697, Wiley Online Library on [29/06/2025]. See the Terms and Conditions (https://onlinelibrary.wiley.com/terms-and-conditions) on Wiley Online Library for rules of use; OA aricles are governed by the applicable Creative

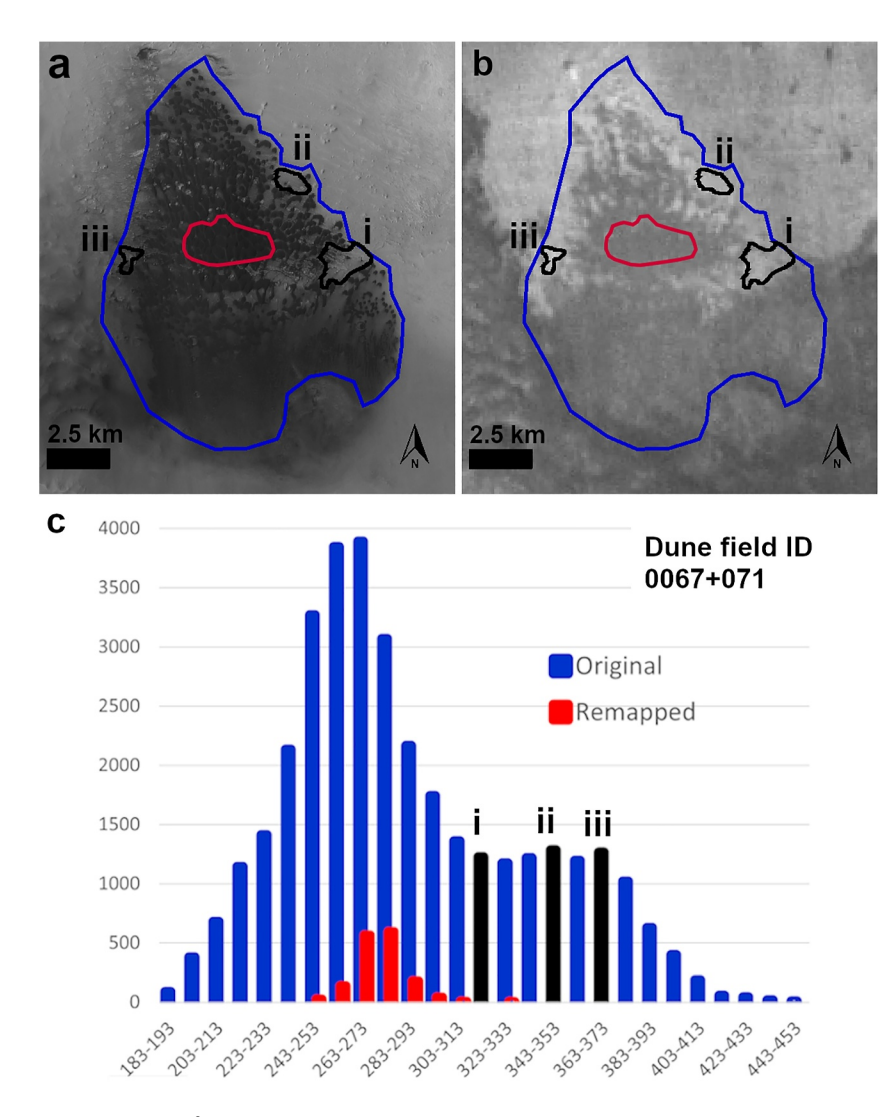


**Figure 2.** Example of an MGD<sup>3</sup> polygon having a bimodal histogram of thermal inertia values within which a sandy area is delineated having a unimodal histogram. (a, b) Dune field 0067 + 071, showing original MGD<sup>3</sup> polygon (blue) and sandy area delineation (red) overlain on (a) CTX mosaic and (b) THEMIS thermal inertia stamps. Lower case Roman numerals refer to three areas of substrate. (s) Histograms of thermal inertia values for the original MGD<sup>3</sup> polygon (blue bars, modes at  $\sim$ 270 and  $\sim$ 365 tiu) and the delineation of the sandy area with dune bedforms (red bars, mode at  $\sim$ 275 tiu). Black bars outline the values for the three substrate areas. Modal values on *x*-axis are in tiu units, ranging from 183 to 193 for the first bar to 443–453 for the last bar; for legibility, every other bar is labeled. Similar plots and images from each of 34 sand areas showing a unimodal histogram are provided in the spreadsheet available as Supporting Information.

a delineation that effectively includes mostly sandy surfaces and excludes most non-sand areas. Delineations that yielded bi- or multimodal histograms were excluded from our work. In our published data set, two dune fields (2763-076 and 3154-078) yielded histograms with a modal value of  $\leq$ 350 tiu from one mapper but modal values of >350 from the other mapper(s). In the Arabia Terra region, a particularly promising site for sand generation (Burr & Finch, 2024), two dune fields (3502 + 047 and 3528 + 080) have modal values within ~10% of the cutoff value of 350 tiu. For completeness and because of regional interest, all eight histograms for these four dune fields are included. We explored ~75 tropical dune fields, delineating sandy areas and collecting data from 54 of them (Figure 1) in order to have a representative sampling. For the dune fields for which sandy areas were delineated by multiple mappers, the data collected by each mapper are individually shown. Each dune field polygon samples data from not only multiple pixels but also multiple thermal inertia images. As the histogram shapes of these thermal inertia values from each dune field were not know a priori, our data include both median and mean values from the sampled THEMIS thermal inertia data.

BURR ET AL. 5 of 17

Than a Single TI Derivation. With Corre of Published Thermal Inertia Values (in Tiu) for Dune Fields With More

	Dune Crater field ID	0194-468 Kaiser	0304-475	0347-437 Rabe	Moreux 0443+417	1370-050	Gale southern Bagnold Dunes	
	Model	Kieffer et al., 1977						<sup>a</sup> Edgett and Christensen, 1991
TI (iu) for single IRTM spots stdev	IRTM / Viking high- res a. 1	339 2 <i>V</i> 335 <i>co</i> 335	343 2 339	335 11 331	347			
	Models	Very coarse sand	Mellon et al., 2000; Jakosky et al., 2000					<sup>b</sup> Fenton et al., 2003
TI (tiu) mean of TES spots (partially overlapping the dune field) stdev	TES / MOC WA <sup>b</sup>		~233 to ~355					
	Model	Medium Putzig and to very Mellon, 2007 coarse sand						'Gullikson et al., 2018
TI (tiu) mean of nighttime TES data (coverage not specified)	TES / MGD <sup>3,e</sup>	448	409	502	240	200		
stdev		52 Medium sand to pebbles	Ξ	ı	ı	1		
	Model					Kieffer, 2013		<sup>d</sup> Edwards et al., 2018
TI (tiu) stdev	THEMIS (117950012) <sup>d</sup>			Medium to coarse	sand	200 to 310 <sup>8</sup>		
	Model	Fergason et al., 2006		se n				this work
TI (tiu): mean of mean values	THEMIS / MGD <sup>3.e</sup>	352	371	379	275	381	3948	<sup>8</sup> from 117950012
Range (mean +/- stdev stdev)		39 313 to 391	25 346 to 396	46 333 to 425	41 234 to 316	84 297 to 465	21 373 to 415	
		Medium to very coarse sand						

Note. In comparison with the range of values derived using the methodology from this work (shown in the most righthand columns), cells with green shading indicate overlap, cells with yellow shading vary by up to ~40% (e.g., Rabe), from very coarse sand to pebbles. For Kaiser, Proctor, and Rabe, individual IRTM data spots are smaller than each dune field as observed in high-resolution Viking imaging. For Moreux, IRTM data spot exceeds the dune field as observed in high-resolution Viking imaging. \*Refers to Edgett and Christensen (1991) in the bottom cell of the "Model" column. \*Prefers to indicate adjacent values, and cells with pink shading indicate no overlap. The total range of values corresponds to a range of grain sizes from medium sand to pebbles. For individual dune fields, values Refers to this work at the bottom of the "Model" column. fmodel updated by Edwards et al. (2018). Frefers to both the values of 200 to 310 and to the value of 394 and indicates that both sets of values Fenton et al. (2003) at the bottom of the "Model" column. Frefers to Gullikson et al. (2018) at the bottom of the "Model" column. <sup>d</sup>refers to Edwards et al. (2018) at the bottom of the "Model" column. were derived from image I17950012. 23335864, 2024, 9, Downloaded from https://agupubs.onlinelibrary.wiley.com/doi/10.1029/2024EA003697, Wiley Online Library on [29/06/2025]. See the Terms and Conditions (https://onlinelibrary.wiley.com/terms-and-conditions) on Wiley Online Library for rules of use; OA articles are governed by the applicable Creative Commons Licensea

BURR ET AL. 6 of 17

At the time of this work, a spatially variable offset between the visible-wavelength mosaic on which we delineated sandy areas (Dickson et al., 2018) and the THEMIS data from which we collected thermal inertia data (Fergason, Christensen, & Kieffer, 2006) added some error into our results. We tested the effect of this offset on one dune field (ID 1284-163) to estimate its order of magnitude effect on our results. In this test, the offset of the sandy delineation using the CTX mosaic versus the THEMIS mosaic showed a ~0.5 km difference. We mitigated this source of error by focusing our work on the larger of the large MGD<sup>3</sup> dune fields (Hayward et al., 2007).

#### 2.4. Assessment of the Potential Influence of Dust on Thermal Inertia Values

Because grain size has a predominant influence on thermal inertia, smaller grains (i.e., dust) decrease the thermal inertia whereas larger sediments or bedrock outcrops increase it (cf., Fergason, Christensen, & Kieffer, 2006). Although we designed our methodology so as to exclude non-sand substrate (e.g., boulders), potential contamination by airborne sediments, that is, dust, is both possible and—given the annual observation of several hundred dust storms on Mars (Cantor et al., 2001)—a likely influence. Thus, in order to estimate the influence of dust on our derived thermal inertia values for Martian dune sand, we quantified the correlation of the thermal inertia values with the dust cover.

The amount of dust cover on Mars has been quantified using a variety of data sets. A dust cover index (DCI; Ruff & Christensen, 2002) was derived from the TES data (global mapping res. 3 km/px; Christensen et al., 2001). A surface dust abundance was also based on TES data (Bandfield, 2002). A dust map was produced with data from the Observatoire pour la Minéralogie, l'Eau, les Glaces et l'Activité (OMEGA) instrument (res. ~300 m to 5 km per pixel; Bibring et al., 2006 and references therein). For this work, which involved analysis of dune field polygon areas down to a few km², we selected the data set with the consistently highest resolution or smallest map pixel scale to gather the largest number of data points over each dune field. Thus, we used the TES DCI in this work. For this index, the average value of  $0.969 \pm 0.007$  corresponds to dust-free surfaces, whereas the average values of  $0.931 \pm 0.009$ , corresponds to dust-covered surfaces.

#### 2.5. Derivation of Grain Sizes

From dust-free thermal inertia values over dune fields, grain sizes may be derived (e.g., Jakosky, 1986 and references therein; Edgett & Christensen, 1991) through relationships of variable complexity and various parameterization (Edwards et al., 2018; Presley & Christensen, 1997a, 1997b; Piqueux & Christensen, 2009). For this work, we used the equation from Presley (2002).

$$\kappa = \left(CP^{2/3}\right) d^{(0.52-K \cdot P)} \tag{1}$$

where  $C \approx 0.0014$ ,  $K \approx 0.01$  for units of W/m K for the thermal conductivity  $\kappa$ , and P is atmospheric pressure in torr. This equation simplifies earlier work (Jakosky et al., 2000; Presley & Christensen, 1997b) through the assumption that the product of density and thermal conductivity is consistently equal to first order to  $1.0 \times 10^6$  J/m<sup>3</sup> K for a "typical" martian atmospheric pressure of 5 torr. From the definition for thermal inertia as  $(\kappa \rho c)^{1/2}$ , that equation may be solved for the grain size, namely:

$$d = (I^2 / 4090)^{1/0.47}.$$
 (2)

With Equation 2, we converted our thermal inertia values to grain sizes.

#### 3. Results

#### 3.1. Thermal Inertia Values for Martian Dune Fields From the Equatorial MGD<sup>3</sup> Data Set

Out of the 73 dune fields in the USGS equatorial dune database within 30 degrees of the equator, we delineated sandy areas within 54 of those dune fields, finding a total of 34 dune fields from which we derived unimodal histograms and modal values consistent with sand. Sand areas that derive from the same dune field are designated with an ordinal position (N, S, etc., for north, south, etc.) of the sand area within the dune field. Because the sandy areas are necessarily a portion of the original MGD<sup>3</sup> polygon (Figure 2), their histograms are comprised of fewer data points. Delineation of sand areas in a single dune field by more than one worker produced limited variability

BURR ET AL. 7 of 17

2335084, 2024, 9, Downloaded from https://agupubs.onlinelibrary.wiley.com/doi/10.1029/2024EA003697, Wiley Online Library on [29/06/2025]. See the Terms and Conditions (https://onlinelibrary.wiley.com/term

and-conditions) on Wiley Online Library for rules of use; OA articles are governed by the applicable Creative Commons

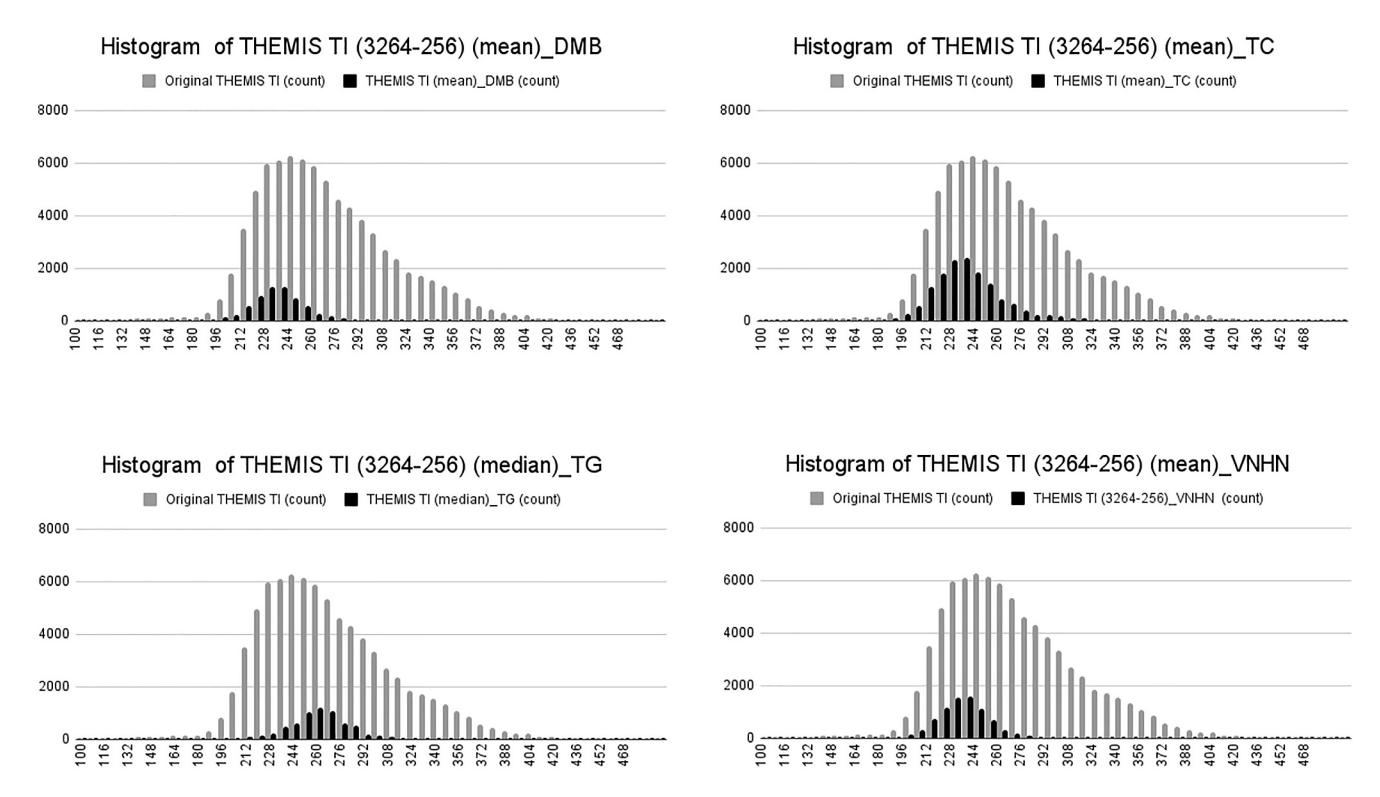


Figure 3. The unimodal histograms of thermal inertia values for sandy areas (shown as dark bars) within Dune Field 3264-256 (shown as Gy bars) as delineated by all four workers, given in alphabetical order, overlain on the histogram of the thermal inertia values for the MGD3 polygon. This example comparison shows that for all four workers (initials in the headers) and for both mean and median values, the modal values of the four histograms are within  $\sim 10\%$  of each other and correspond to fine to medium sand. Thermal inertial values (x-axes) range from 100 to 468 tiu; counts (y-axes) range from 0 to 8000. Similar plots from each of 34 sand areas for a total of 69 histograms are provided in Supporting Information with quantitative information available in Table 2.

among our results (Figure 3). Our total data set of 69 sand-only areas is given as quantitative values (Table 2) and plots (see Supplemental Information S1).

#### 3.2. Context From Previously Derived Thermal Inertia Values for Martian Dune Fields

In developing context for our work and previously derived thermal inertia values, we focus on dune fields with more than a single previous publication of thermal inertia values. Thermal inertia values were previously published for 58 dune fields in the equatorial MGD<sup>3</sup> database (Gullikson et al., 2018). Of those dune fields, additional thermal inertia values had been derived for dune fields within the southern mid-latitude craters of Kaiser (0194–468), Proctor (0297–476), and Rabe (0347–437) and the northern mid-latitude Moreux crater (0443 + 417), whose dune field IDs (in parentheses) indicate the east longitude to a tenth of a degree and latitude to a tenth of a degree (see Hayward et al., 2007). Thermal inertia has also been estimated from orbital data for the southern portion of the Bagnold dune field (itself a portion of MGD<sup>3</sup> dune field 1370-050). We rederived thermal inertia values for those five locations using the method described above. In addition, we visually reproduced the outline of the southern Bagnold dunes within which thermal inertia values were previously derived (Edwards et al., 2018) and collected data for that area both from all overlapping THEMIS thermal inertia stamps (as per the method described above) and from the single THEMIS stamp (I17950012) used in the previous work (Edwards et al., 2018) though without the special processing or modeling applied to it in that work; that is, we collected data from I17950012 as processed by Fergason, Christensen, & Kieffer, 2006.

For these six locations, previously derived thermal inertia data show a range of values, both for the compiled data set as a whole and for individual dune fields (Table 1). From the earliest thermal model (Kieffer et al., 1977), IRTM data for the Kaiser, Proctor, Rabe, and Moreux crater dune fields yielded values in the mid-300's in tiu (Edgett & Christensen, 1991). From a different thermal model (Jakosky et al., 2000; Mellon et al., 2000), TES input data for the Proctor crater field gave values of ~233 to ~355 tiu, overlapping the IRTM data though with a wider range to lower values. A subsequent, broader, study based also on TES data but using a more advanced

BURR ET AL. 8 of 17

23355084, 2024, 9, Downloaded from https://agupubs.onlinelibrary.wiley.com/doi/10.1029/2024EA003697, Wiley Online Library on [29/06/2025]. See the Terms and Conditions (https://onlinelibrary.wiley.com/terms-and-conditions) on Wiley Online Library for rules of use; OA articles are governed by the applicable Creative Commons License



 Table 2

 Compilation of Data of Delineated Areas Within MGD³ Dune Fields That Show a Unimodal Histogram and Mode  $<\sim$ 350  $\mu$ m, Along With Grain Size Classifications and Average and Standard Deviations for Specific Geographic Regions

Sand areas as dune ID	Worker initials	Mode	Estimated grain size (µm) (from modal value)	Grain size classification (from modal value)	Geographic region	Average of modal regional grain sizes (µm)	Standard deviation of regional modal grain size (µm)
0067 + 071	VNHN	258	378	Medium sand			
	TG	269	451	Medium sand			
0570-021	VNHN	220	192	Fine sand	SYRTIS MAJOR/	556	362
0628 + 266	VNHN	337	1179	V. Coarse sand	NILI PLANA		
0671 + 088	VNHN	231	236	Fine sand			
	TG	235	254	Medium sand			
0755 + 207	VNHN	295	669	Coarse sand			
	TG	308	803	Coarse sand			
937-089	VNHN	296	679	Coarse sand			
TC	TC	297	688	Coarse sand			
	TG	285	160	Fine sand			
249-136	VNHN	263	410	Medium sand	NORTHERN	405	349
	TC	200	128	Fine sand	TERRA		
	TG	289	612	Coarse sand	CIMMERAI		
1284-163_E	VNHN	237	264	Medium sand			
	TC	237	264	Medium sand			
284-163_W	VNHN	271	466	Medium sand			
	TC	271	466	Medium sand			
286-143	VNHN	200	128	Fine sand			
	TC	210	158	Fine sand			
	TG	211	160	Fine sand			
370-050	VNHN	297	688	Coarse sand			
	TC	281	544	Coarse sand			
	TG	261	236	Fine sand			
375-177	VNHN	311	838	Coarse sand			
	TC	311	838	Coarse sand			
	TG	242	287	Medium sand			
593 + 111	VNHN	212	164	Fine sand			
	TG	231	236	Fine sand			
2763-076	VNHN	361	1579	V. Coarse sand	IUS	1532	235
	TC	340	1224	V. Coarse sand			
	TG	372	1794	V. Coarse sand			
2886-131_S	VNHN	350	1385	V. Coarse sand	MELAS	1065	385
	TC	333	1120	V. Coarse sand			
901-101	VNHN	267	438	Medium sand			
	TC	291	631	Coarse sand			
908-105	TG	349	1368	V. Coarse sand			
2908-105_S	VNHN	346	1318	V. Coarse sand			
	TC	338	1194	V. Coarse sand			
2971-046_S	VNHN	299	708	Coarse sand	JUVENTAE	708	0
3023-155	VNHN	294	659	Coarse sand	COPRATES	930	168
	TG	333	1120	V. Coarse sand			

BURR ET AL. 9 of 17

# **Earth and Space Science**

Table 2

Sand areas as dune ID	Worker initials	Mode	Estimated grain size (μm) (from modal value)	Grain size classification (from modal value)	Geographic region	Average of modal regional grain sizes (µm)	Standard deviation of regional modal grain size (µm)
3025-144	VNHN	322	971	Coarse sand			
	TC	322	971	Coarse sand			
3076-032	VNHN	297	688	Coarse sand			
	TG	301	728	Coarse sand			
3113-068_N VN	VNHN	300	719	Coarse sand	GANGES (with	756	424
	TC	243	293	Medium sand	3134-004)		
3113-068_S	VNHN	315	884	Coarse sand			
	TC	319	933	Coarse sand			
	TG	344	1286	V. Coarse sand			
3120-070	VNHN	257	372	Medium sand			
	TC	276	504	Coarse sand			
	TG	264	417	Medium sand			
3124-080_E	VNHN	301	729	Coarse sand			
	TC	283	561	Coarse sand			
3134-004	VNHN	212	164	Fine sand			
3154-078	VNHN	350	1385	V. Coarse sand			
	TC	361	1579	V. Coarse sand			
3264-256	VNHN	241	283	Medium sand	(western) ARABIA	1019	667
	TC	307	793	Coarse sand	TERRA		
	DMB	241	283	Medium sand			
	TG	250	330	Medium sand			
3443 + 084_E	VNHN	355	1471	V. Coarse sand			
3487 + 005	VNHN	305	771	Coarse sand			
	TG	282	552	Coarse sand			
3502 + 047	VNHN	373	1815	V. Coarse sand			
3528 + 080	VNHN	376	1878	V. Coarse sand			
	TG	382	2009	Granules			
0067 + 071	VNHN	258	378	Medium sand			
	TG	269	451	Medium sand			

Note. For a version of this table with images of each sand-only area, see SI Table with sand classification and images.

thermal model (Putzig & Mellon, 2007) resulted in generally higher thermal inertia values—within the 400's of tiufor the Kaiser, Procto-r, and Rabe crater dune fields (Gullikson et al., 2018), although the large standard deviation for the Proctor crater dune field cause its range of thermal inertia values to overlap those of both previous studies. For the northern hemisphere Moreux crater, values were offset to the mid-200's of tiu. TES data for the equatorial Gale crater dune field gave a value of 500 tiu, whereas analysis of a single nighttime THEMIS cube processed with an updated thermal model (Kieffer, 2013) yielded values for the southern portion of the Bagnold Dunes of 200-310 tiu (Edwards et al., 2018).

The following are several reasons for the variation in these data. Different pixel resolutions of the thermal data necessarily lead to inclusion of different materials, with high resolutions commonly enabling collection of data more likely (though not necessarily) to be co-located within the dune field. Different thermal models, with generally increasing sophistication of, for example, atmospheric removal, inclusion of layering effects, are other fundamental sources of the variation in these published results, as are the (assumed/measured) input into those

BURR ET AL. 10 of 17

23335084, 2024, 9, Downloaded from https://agupubs.onlinelibrary.wiley.com/doi/10.1029/2024EA003697, Wiley Online Library on [29/06/2025]. See the Terms and Conditions

-conditions) on Wiley Online Library for rules of use; OA articles are governed by the applicable Creative Commons

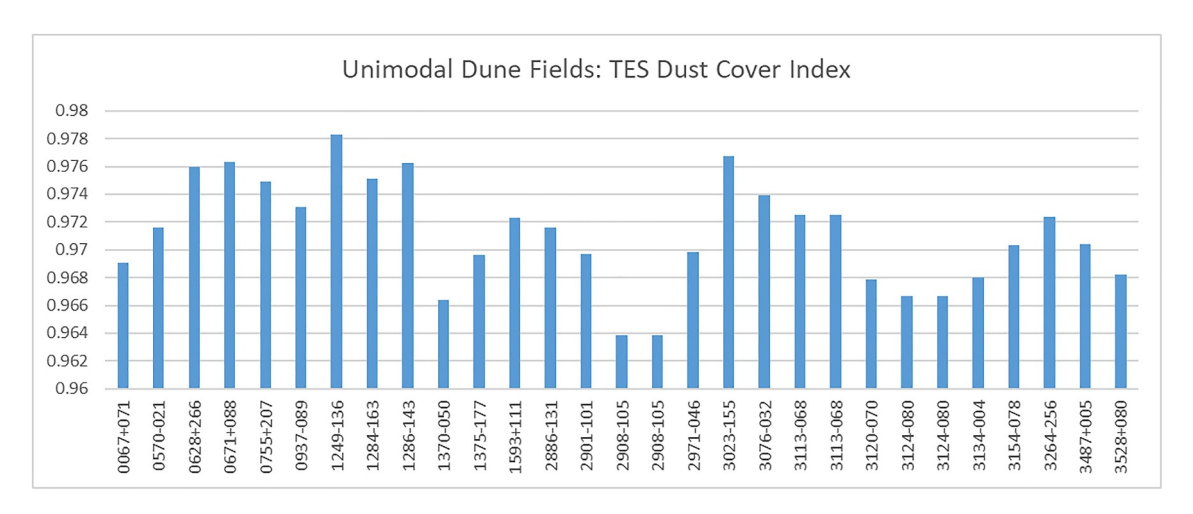


Figure 4. Plot of average TES dust cover index values for each dune field with an interior unimodal sandy area. As DCI values of  $>0.969 \pm 0.007$  correspond to dust-free surfaces, these values of 0.964-0.978 indicate that all of these sand areas are generally dust-free.

models. Proctor crater (Fenton et al., 2003) and possibly the other three mid-latitude craters (e.g., Schorghofer & Edgett, 2006) experience seasonally variable frost, which could account for some of the significant variation between the IRTM-based values (Edgett & Christensen, 1991) and the TES-based values (Fenton, 2005; Gullikson et al., 2018). Other surface influences include dust, cementation (Piqueux & Christensen, 2009), and surface heterogeneities (Putzig & Mellon, 2007).

This compilation of previous thermal inertia values in comparison to values derived in this work shows frequent agreement. Our results are consistent with the IRTM-based results (Edgett & Christensen, 1991) for the three southern hemisphere crater dune fields in Kaiser and Rabe and (within 1 tiu) Proctor craters. Subsequent values for Proctor crater (Fenton et al., 2003) overlap with ours. Although the thermal inertia values from the IRTM (Edgett & Christensen, 1991) for the northern hemisphere Moreux crater dune field are higher than ours, the value from a subsequent TES-based study (Gullikson et al., 2018) falls within our range of values.

Surprisingly to us, our results for the southern Bagnold dune field derived from THEMIS stamp I17950012 (from Fergason, Christensen, & Kieffer, 2006) are higher than those previously published (Edwards et al., 2018) for this specific locale and using this specific THEMIS stamp. We speculate that difference is due to (a) the specialized processing of that stamp and (b) the difference in the applied thermal model. Conversely, the thermal inertia values derived here using all overlapping THEMIS stamps for the entire western Gale crater dune field (1379-050) of which Bagnold dunes is the northern part overlap the values for the southern Bagnold dunes from THEMIS stamp I17950012 (Edwards et al., 2018).

Overall, these published thermal inertia values for dune fields on Mars are variable, both in value and in the inferred grain size. Our data for sandy areas within dune fields, drawn from a globally available data set (Fergason, Christensen, & Kieffer, 2006), fall within the range of these published dune field values. We consider this comparison to show the validity our results from these six locales and by extension for the other sand areas in this study. With this contextualization, we next describe the potential influence of dust.

#### 3.3. Analysis of Dust Influence on Derived Thermal Inertia Values

Values from the DCI for the unimodal sandy areas range from 0.964 to 0.978 (Figure 4). As an average DCI value of  $0.969 \pm 0.007$  corresponds to dust-free surfaces (Ruff & Christensen, 2002), these results show that the sand areas in this study are generally dust free, indicating that the thermal inertia values are not excessively influenced by dust cover.

#### 3.4. Derived Grain Sizes

Based on these findings of consistency with prior published work and minimal dust influence, we converted the modal values of our unimodal histograms to grain sizes (Figure 5, Table 2). These results show a range of sand

BURR ET AL. 11 of 17

23335084, 2024, 9, Downloaded from https://agupubs.onlinelibrary.wiley.com/doi/10.1029/2024EA003697, Wiley Online Library on [29/06/2025]. See the Terms and Conditions (https://onlinelibrary.wiley

litions) on Wiley Online Library for rules of use; OA articles are governed by the applicable Creative Co

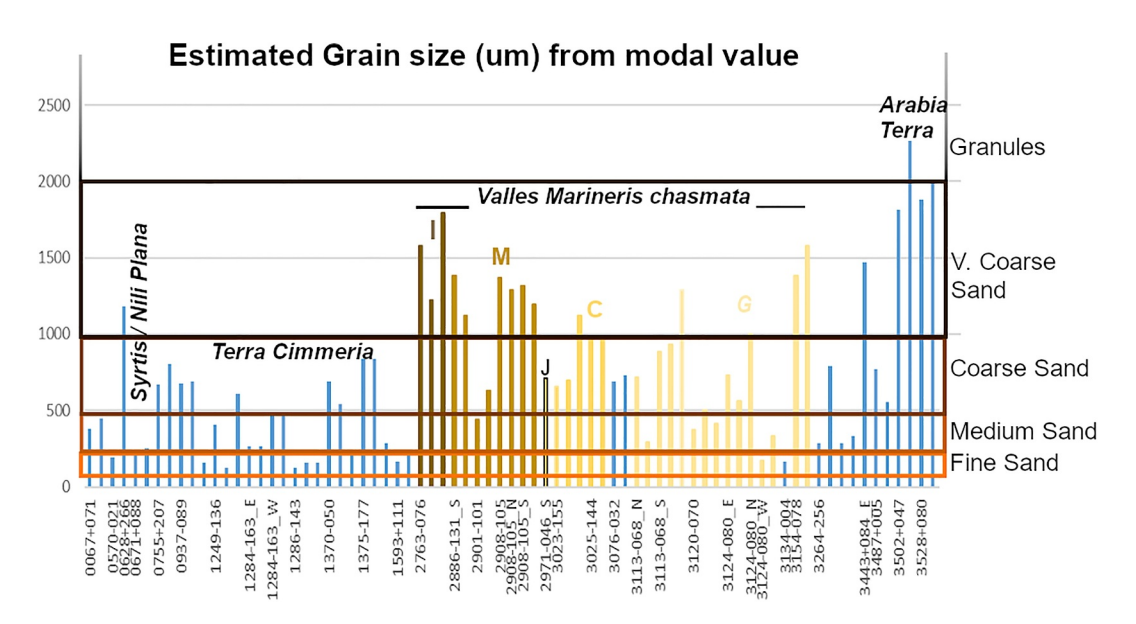


**Figure 5.** Estimated grain sizes derived from modal thermal inertia values for the sandy areas. Vertical bars to the right of a Dune Field ID (on the *x*-axis) refer to sand areas within that dune field as characterized by multiple workers. These results show grain classifications from fine sand to granules and point toward geographically characteristic ranges of values. Non-italicized letters indicate data from the Ius, Melas, Juventae, Coprates, and Ganges chasmata. To view the data in this figures, see Table S1 with sand classification and images.

size classes, from fine sand up to granules. The distribution of classifications is approximately symmetric, with the modal classification as coarse sand (27 classifications), equal numbers of medium and very coarse sand (17 classifications each), and 12 classifications of fine sand versus two classifications as granules (2–4 mm; Fenton et al., 2003).

#### 4. Discussion

#### 4.1. Longitudinal Clustering of Sand Size Characteristics

The grain size results suggest a characteristic range of grain size values for different geographic locations. Sand grain sizes inferred from modal values for Syrtis Major and the Nili Planum region (average grain size of 556 µm, standard deviation of 362 µm) range from a single inference of fine sand up to a single inference of very coarse sand. Sand sampled within Hesperia Planum (average grain size of 405 µm, standard deviation of 349 µm) has a more narrow range of classifications, from several fine to several coarse sand sizes. In comparison, the range of sand sampled within the Valles Marineris chasmata dune fields is shifted to larger grain classes, ranging from medium to very coarse sand sizes. Although our methodology differs from that employed by Chojnacki, Burr, & Moersch, 2014 for estimating particle sizes, our modal values from Ius, Melas, Juventae, Coprates, and Ganges chasmata fall within the ranges from that previous work. The results of our sampling of Valles Marineris dune fields point toward some clustering of values by chasmata. The largest inferred grain sizes occur in the west in Ius Chasma (average grain size of 1532 μm, standard deviation of 235 μm). To the east, sizes decrease in the dune fields of Melas chasma (average grain size of 1092 µm, standard deviation of 368 µm). The three eastern chasmata —, a single datum in Juventae chasm (average grain size of 708 μm), Coprates Chasma (average grain size of 884 μm, standard deviation of 177 μm), and Ganges Chasma dune fields (average grain size of 708 μm, standard deviation of 424 µm)—show similar average grain sizes. Of all the sampled dune fields, those in western Arabia Terra (average grain size of 1132 µm, standard deviation of 730 µm) have the largest maximum inferred grain classification of granules, along with several sites of very coarse sand.

#### 4.2. Potential Inferences for Sand Production Mechanisms

Sand sources identified to date on Mars has all been local to sand dunes. Some sand in the Valles Marineris is sourced from wall rock (Chojnacki, Burr, Moersch, et al., 2014). In the mid-southern latitudes, numerous dune fields lie between and within southern highlands craters that provide this sediment (Fenton, 2005; Tirsch

BURR ET AL. 12 of 17

23335084, 2024, 9, Downloaded from https

.com/doi/10.1029/2024EA003697, Wiley Online Library on [29/06/2025]. See the Terms

et al., 2011). Gypsum-rich sand forms an erg around the North Polar Layered Deposits, the inferred source of this compositionally distinctive sand (Fishbaugh et al., 2007; Langevin et al., 2005). Deposits within single craters, whether studied with landed (e.g., Greeley et al., 2008) or orbital data (e.g., Cardinale et al., 2020; Fenton et al., 2003), are also inferred to be locally sourced. Local pathways have also been inferred within craters (Cardinale et al., 2020; Greeley et al., 2008).

Given a likelihood of local sand sources in general along with the demonstration of local sand source in Valles Marineris, this suggestion in our data of clustering of sand sizes by geographic region, if correct, would imply regional sand production mechanisms that yield different grain sizes. Volcanism has been suggested to produce sand grains (e.g., Greeley & Iversen, 1985), both through breakdown of effusive material (epiclastic grains) and through explosive volcanism (pyroclastic grains), consistent with basaltic sand production on Earth (Edgett & Lancaster, 1993 and references therein). Pyroclastic sand has been inferred in the Aeolis Dorsa region, with derived grain sizes up to 1.80 mm (Burr et al., 2022). The Arabia Terra region is inferred to have hosted explosive volcanoes (Michalski & Bleacher, 2013) that distributed pyroclastic deposits regionally (Whelley et al., 2021). That Arabia Terra exhibits the largest maximum grain sizes consistently >1 mm suggests a pyroclastic sand source that produced large grains. In comparison, the Valles Marineris wall sources for the chasmata dune fields (Chojnacki, Burr, Moersch, et al., 2014) would be smaller epiclastic grains formed by erosion of the flood lavas comprising the layering in chasmata walls (McEwen et al., 1999).

#### 4.3. Comparison With Sand Flux Data

Qualitative comparison of these inferred grain sizes with published sand flux data (Chojnacki et al., 2019) are also suggestive. Whereas the inferred grain sizes for the Syrtis Major region are some of the smallest in this tropical dunes data set, that region has some of the globally highest published sand-flux values. The sampled dune fields of northern Terra Cimmeria and the Valles Marineris chasmata continue that relative trend, showing larger grain sizes and lower sand flux values than Syrtis Major.

This comparison, pointing toward an inverse relationship between grain size and sand flux, suggests that larger grain sizes might be moved more slowly. That is, heavier grains result in lower sand flux, as implied by grain size threshold curves (e.g., Greeley & Iversen, 1985; Kok et al., 2012). Such a relationship would imply a transport regime in these lower flux regions, in which the sand flux is limited by the regional wind speeds.

Arabia Terra, which has the largest maximum grain sizes, does not fit this trend, as the measured sand flux (for those sampled dune fields) is similar to the flux in Terra Cimmeria and Valles Marineris, which have smaller inferred grain sizes. This relative relationship suggests a regime in which transport is limited by large sand sizes.

#### 5. Summary and Future Work

In this work, we have developed a freeware-based methodology to infer grain sizes of sand dunes from thermal inertia data in sand dunes on Mars. Having contextualized the utility of this approach in comparison with prior inferences of dune grains sizes, we applied our methodology to tropical dune fields, finding a range of grain sizes that loosely clustered by geographic region. Comparison of our results to published sand flux modeling suggests an approach for distinguishing locations of sand transport limited by wind energy from locations of sand transport limited by sand grain sizes. A more global and qualitative comparison of estimated grain sizes versus inferred sand fluxes would test this suggestion.

The intentionally accessible methodology developed in this work enables a variety of future endeavors building on and expanding from this effort, as do improvements in existing data sets. As noted above, an offset existed at the time of the data collection for this work between the CTX and THEMIS global mosaics. Since that time, a new CTX mosaic has been released for which the tiles within 60° of the equator are registered to the THEMIS-controlled IR mosaic (Dickson et al., 2023). Although we assert that the error introduced into our data by this mismatch is not significant given our use of the grain size distribution to check for unimodality (Section 2.3), future use of this next CTX mosaic would further minimize such offset error.

The compilation of previously published thermal inertia results for dune fields, in particular the disparate results for the southern Bagnold dune field from the same THEMIS image (Section 3.2), points to the importance of the thermal data and model for deriving thermal inertia values. An explanation of this range of values for the same dune fields and (for the Bagnold dunes) even the same area within the field would benefit from a more global

BURR ET AL. 13 of 17

23335084, 2024, 9, Downloaded from https://agupubs.onlinelibrary.wiley.com/doi/10.1029/2024EA003697, Wiley Online Library on [29/06/2025]. See the Terms and Conditions (https://onlinelibrary.wiley

analysis, work that would be facilitated by the accessible method developed here for collecting dune sand thermal inertia values. Whereas the thermal model used to derive thermal inertia data from the THEMIS nighttime image is updated from previous work (Fergason, Christensen, & Kieffer, 2006), a model of thermal inertia values from the THEMIS data set has published (Ciazela et al., 2021) as has a recent mosaic of Martian thermal inertia data from the Mars Climate Sounder (Piqueux et al., 2023). Should those more recent data become available within JMARS, future work using those data with the methodology outlined here could provide more overall accurate results

Whereas we confined our methodological development strictly to tropical dune fields, future work could expand this range to more poleward latitudes, for which comparative data exist (Gullikson et al., 2018). This latitudinal expansion would both provide a second look at higher resolutions of the thermal inertia of these mid-latitude dune fields, thereby improving our characterization of their grain sizes across geographic and climatic regions and enabling more accurate assessment of differences among those pervasive deposits of grain characteristics.

Lastly, this work provides a foundation for future investigations into mineralogical correlations with dune field and grain sizes. Whereas olivine has been suggested to be a positive influence on thermal inertia (e.g., Bandfield & Rogers, 2008; Hamilton et al., 2003), the data to date have been inconclusive (e.g., Brown et al., 2020; Hanna et al., 2016). The accessible methodology demonstrated here provides an efficient path to further exploration of this complex relationship between mineralogy and thermal inertia and in general to better understanding the thermal inertia of dune sand on Mars.

#### **Conflict of Interest**

The authors declare no conflicts of interest relevant to this study.

#### **Data Availability Statement**

All data analyzed in this work are available through the NASA Planetary Data System and through the Java Mission-planning and Analysis for Remote Sensing (jmars.asu.edu) geospatial information system software. A JMARS session file ("Burr\_et al.\_ESS.jmars") is available as Supporting Information that includes:

- 1. A JMARS layer file "Tropical-dune-fields-with-sand-areas-having-unimodal-histograms" showing as polygons the sand-only areas delineated from the USGS EQ Mars Dune Fields between 30°N and 30°S analyzed in this work from which we derived unimodal histograms
- 2. A JMARS layer file "Tropical-dune-fields-with-sand-areas-having-multimodal-histograms" showing as points those USGS EQ Mars Dune Fields between 30°N and 30°S analyzed in this work, from which we derived multimodal histograms
- 3. The USGS EQ Mars Dune Database at 50% opacity
- 4. The CTX Global Mosaic as the data on which the delineations were made

The Supporting Information document describes the Methodology used to collect data from the NASA Planetary Data Systems data using the JMARS software.

The data collected from the NASA Planetary Data Systems data using the JMARS software (Burr et al., 2024) consist of thermal inertial values, presented in the form of histograms, for sand-only areas of dune fields from the USGS Equatorial MGD<sup>3</sup>. As described in the manuscript above, unimodal histograms with a model  $\leq$ 350 tiu are considered to represent sand-only areas, and a zip archive of those histograms ("Unimodal Histograms") is available at https://openknowledge.nau.edu/id/eprint/6256/ along with a Readme file describing the collected data.

## Acknowledgments

This work was conducted at Northern Arizona University (Flagstaff, Arizona), which sits on homelands sacred to the Hohokam Diné, Hopi, Western Apache, and other Native peoples. We honor the past, present, and future generations of these tribes on their ancestral lands. VNHN and TC were supported in this work by the NAU Interns to Scholar program and TG was supported by the NAU Astronomy and Planetary Science Research Experience for Undergraduates program. Two anonymous reviews and editorial suggestions improved this manuscript.

#### References

Ahlbrandt, T. S. (1979). Textural parameter of eolian deposits. In E. D. McKee (Ed.), A study of global sand seas (Vol. 1052, pp. 21–51). U.S. Geological Survey Paper. Chapter B.

Ahlbrandt, T. S., & Fryberger, S. G. (1981). Sedimentary features and significance of interdune deposits. In F. G. Ethridge & R. M. Flores (Eds.), Recent and ancient nonmarine depositional environments: Models for exploration. https://doi.org/10.2110/pec.81.31

Bandfield, J. L. (2002). Global mineral distributions on Mars. *Journal of Geophysical Research*, 107(E6). https://doi.org/10.1029/2001JE001510
Bandfield, J. L., & Rogers, A. D. (2008). Olivine dissolution by acidic fluids in Argyre Planitia, Mars: Evidence for a widespread process?

Geology, 36(7), 579–582. https://doi.org/10.1130/g24724a.1

Bibring, J.-P., Langevin, Y., Mustard, J. F., Poulet, F., Arvidson, R., Gendrin, A., et al. (2006). Global mineralogical and aqueous Mars history derived from OMEGA/Mars express data. *Science*, 312(5772), 400–404. https://doi.org/10.1126/science.1122659

BURR ET AL. 14 of 17

- Bourke, M. C., Edgett, K. S., & Cantor, B. A. (2008). Recent aeolian dune change on Mars. Geomorphology, 94(1-2), 247-255. https://doi.org/10.1016/j.geomorph.2007.05.012
- Bridges, N. T. (1994). Elevation-Corrected thermal inertia and derived particle size on Mars and implications for the Tharsis Montes. *Geophysical Research Letters*, 21(9), 785–788. https://doi.org/10.1029/94GL00368
- Bridges, N. T., Ayoub, F., Avouac, J. P., Leprince, S., Lucas, A., & Mattson, S. (2012). Earth-like sand fluxes on Mars. *Nature*, 485(7398), 339–342. https://doi.org/10.1038/nature11022
- Bridges, N. T., Bourke, M. C., Geissler, P. E., Banks, M. E., Colon, C., Diniega, S., et al. (2012). Planet-wide sand motion on Mars: Geology. *Geology*, 40(1), 31–34. https://doi.org/10.1130/g32373.1
- Brown, A. J., Viviano, C. E., & Goudge, T. A. (2020). Olivine-carbonate mineralogy of the Jezero Crater region. *Journal of Geophysical Research: Planets*, 125(3), e2019JE006011. https://doi.org/10.1029/2019JE006011
- Burr, D. M., & Finch, J. A. (2024). Seeking sand origins on Mars: Towards testing the volcaniclastic hypothesis globally. *Icarus*, 420, 116194. https://doi.org/10.1016/j.icarus.2024.116194
- Burr, D. M., Nguyen, V. N. H., Gibson, T. M.-G., & Chinchkhede, T. (2024). Estimating grain sizes of Martian dune sand: A freeware-based methodology with initial results [Dataset]. https://openknowledge.nau.edu/id/eprint/6256/
- Burr, D. M., Viviano, C. E., Michaels, T. I., Chojnacki, M., & Jacobsen, R. E. (2022). An explosive volcanic origin identified for dark sand in Aeolis Dorsa, Mars. Geology, 50(8), 939–943. https://doi.org/10.1130/g49814.1
- Cantor, B. A., James, P. B., Caplinger, M., & Wolff, M. J. (2001). Martian dust storms: 1999 Mars orbiter Camera observations. *Journal of Geophysical Research*, 106(E10), 23653–23687. https://doi.org/10.1029/2000JE001310
- Cardinale, M., Pozzobon, R., Tangari, A. C., Runyon, K., Di Primio, M., & Marinangeli, L. (2020). Reconstruction of the sand transport pathways and provenance in Moreux crater, Mars. *Planetary and Space Science*, 181, 104788. https://doi.org/10.1016/j.pss.2019.104788
- Chase, S. C., Engel, J. L., Eyerly, H. W., Kieffer, H. H., Palluconi, F. D., & Schofield, D. (1978). Viking infrared thermal mapper. *Applied Optics*, 17(8), 1243–1251. https://doi.org/10.1364/AO.17.001243
- Chojnacki, M., Banks, M. E., Fenton, L. K., & Urso, A. C. (2019). Boundary condition controls on the high-sand-flux regions of Mars. *Geology*, 47(5), 427–430. https://doi.org/10.1130/g45793.1
- Chojnacki, M., Burr, D. M., & Moersch, J. E. (2014). Valles Marineris dune fields as compared with other Martian populations: Diversity of dune compositions, morphologies, and thermophysical properties. *Icarus*, 230, 96–142. https://doi.org/10.1016/j.icarus.2013.08.018
- Chojnacki, M., Burr, D. M., Moersch, J. E., & Wray, J. J. (2014). Valles Marineris dune sediment provenance and pathways. *Icarus*, 232(0), 187–219. https://doi.org/10.1016/j.icarus.2014.01.011
- Christensen, P. R., Bandfield, J. L., Bell, J. F., Gorelick, N., Hamilton, V. E., Ivanov, A., et al. (2003). Morphology and composition of the surface of Mars: Mars Odyssey THEMIS results. Science, 300(5628), 2056–2061. https://doi.org/10.1126/science.1080885
- of Mars: Mars Odyssey THEMIS results. Science, 300(5628), 2056–2061. https://doi.org/10.1126/science.1080885 Christensen, P. R., Bandfield, J. L., Hamilton, V. E., Ruff, S. W., Kieffer, H. H., Titus, T. N., et al. (2001). Mars global surveyor thermal emission
- christensen, P. R., Bandried, J. L., Hamilton, V. E., Ruff, S. W., Kleffer, H. H., 11tus, 1. N., et al. (2001). Mars global surveyor mermal emission spectrometer experiment: Investigation description and surface science results. *Journal of Geophysical Research: Planets*, 106(E10), 23165–23945. https://doi.org/10.1029/2000JE001370
- Christensen, P. R., Engle, E., Anwar, S., Dickenshied, S., Noss, D., Gorelick, N., & Weiss-Malik, M. (2009). *JMARS—A planetary GIS*. American Geophysical Union, Fall Meeting 2009. abstract id.IN22A-06.
- Christensen, P. R., Jakosky, B. M., Kieffer, H. H., Malin, M. C., McSween, H. Y., Nealson, K., et al. (2004). The thermal emission imaging system (THEMIS) for the Mars 2001 Odyssey mission. Space Science Reviews, 110(1), 85–130. https://doi.org/10.1023/b:spac.0000021008.16305.94
- Ciazela, M., Ciazela, J., & Pieterek, B. (2021). High resolution apparent thermal inertia mapping on Mars. *Remote Sensing*, 13(18), 3692. https://doi.org/10.3390/rs13183692
- Cox, R., & Lowe, D. R. (1995). A conceptual review of regional-scale controls on the composition of clastic sediment and the co-evolution of continental blocks and their sediment cover. *Journal of Sedimentary Research*, 65, 1–12. https://doi.org/10.1306/D4268009-2B26-11D7-8648000102C1865D
- Dickson, J. L., Ehlmann, B. L., Kerber, L. H., & Fassett, C. I. (2023). Release of the global CTX mosaic of Mars: An experiment in information-preserving image data processing. 54th Lunar and Planetary Science Conference. Abstract #2353. https://www.hou.usra.edu/meetings/lpsc2023/pdf/2353.pdf
- Dickson, J. L., Kerber, L. A., Fassett, C. I., & Ehlmann, B. L. (2018). A global, blended CTX mosaic of Mars with vectorized seam mapping: A new mosaicking pipeline using principles of non-destructive image editing. 49th Lunar and Planetary Science Conference: Houston. Lunar and Planetary Institute. Abstract #2480.
- Diniega, S., Burr, D. M., Chojnacki, M., Lapôtre, M. G. A., & Swann, C. (2022). Martian dunes: A crucial record of present and past Mars surface environment and Aeolian processes. In J. F. Shroder (Ed.), *Treatise on geomorphology* (2nd ed., pp. 617–636). Academic Press.
- Edgett, K. S., Banham, S. G., Bennett, K. A., Edgar, L. A., Edwards, C. S., Fairén, A. G., et al. (2020). Extraformational sediment recycling on Mars. *Geosphere*, 16(6), 1508–1537. https://doi.org/10.1130/ges02244.1
- Edgett, K. S., & Christensen, P. R. (1991). The particle size of Martian aeolian dunes. *Journal of Geophysical Research*, 96(E5), 22765–22776. https://doi.org/10.1029/91je02412
- Edgett, K. S., & Christensen, P. R. (1994). Mars aeolian sand: Regional variations among dark-hued crater floor features. *Journal of Geophysical Research*, 99(E1), 1997–2018. https://doi.org/10.1029/93je03094
- Edgett, K. S., & Lancaster, N. (1993). Volcaniclastic aeolian dunes: Terrestrial examples and application to Martian sands. *Journal of Arid Environments*, 25(3), 271–297. https://doi.org/10.1006/jare.1993.1061
- Edwards, C. S., Piqueux, S., Hamilton, V. E., Fergason, R. L., Herkenhoff, K. E., Vasavada, A. R., et al. (2018). The thermophysical properties of the Bagnold dunes, Mars: Ground-truthing orbital data. *Journal of Geophysical Research: Planets*, 123(5), 1307–1326. https://doi.org/10.1029/2017JE005501
- Ewing, R. C., Peyret, A.-P. B., Kocurek, G., & Bourke, M. (2010). Dune field pattern formation and recent transporting winds in the Olympia Undae Dune Field, north polar region of Mars. *Journal of Geophysical Research*, 115(E8). https://doi.org/10.1029/2009je003526
- Fenton, L. K. (2005). Potential sand sources for the dune fields in Noachis Terra, Mars. Journal of Geophysical Research E: Planets, 110(11), 1–27. Article Number E11004. https://doi.org/10.1029/2005je002436
- Fenton, L. K. (2020). Updating the global inventory of dune fields on Mars and identification of many small dune fields. *Icarus*, 352, 114018. https://doi.org/10.1016/j.icarus.2020.114018
- Fenton, L. K., Bandfield, J. L., & Ward, A. W. (2003). Aeolian processes in Proctor Crater on Mars: Sedimentary history as analyzed from multiple data sets. *Journal of Geophysical Research*, 108(E12), 5129. https://doi.org/10.1029/2002je002015
- Fenton, L. K., Gullikson, A. L., Hayward, R. K., Charles, H., & Titus, T. N. (2019). The Mars global digital dune database (MGD3): Global patterns of mineral composition and bedform stability. *Icarus*, 330, 189–203. https://doi.org/10.1016/j.icarus.2019.04.025

BURR ET AL. 15 of 17

- Fenton, L. K., & Hayward, R. K. (2010). Southern high latitude dune fields on Mars: Morphology, aeolian inactivity, and climate change. Geomorphology, 121(1-2), 98-121. https://doi.org/10.1016/j.geomorph.2009.11.006
- Fergason, R. L., Christensen, P. R., & Kieffer, H. H. (2006). High-resolution thermal inertia derived from the thermal emission imaging system (THEMIS): Thermal model and applications. *Journal of Geophysical Research E: Planets*, 111(E12). Article Number E12004. https://doi.org/10.1029/2006je002735
- Fergason, R. L., Herkenhoff, K. E., Kieffer, H. H., Christensen, P. R., Bell, I. J. F., & Golombek, M. P. (2006). Physical properties of the Mars Exploration Rover landing sites as inferred from Mini-TES-derived thermal inertia. *Journal of Geophysical Research E: Planets*, 111(E2). Article Number E02S21. https://doi.org/10.1029/2005je002583
- Fishbaugh, K. E., Poulet, F., Chevrier, V., Langevin, Y., & Bibring, J.-P. (2007). On the origin of gypsum in the Mars north polar region. *Journal of Geophysical Research*, 112(E7), E07002. https://doi.org/10.1029/2006je002862
- Gómez-Elvira, J., Armiens, C., Castañer, L., Domínguez, M., Genzer, M., Gómez, F., et al. (2012). REMS: The environmental sensor suite for the Mars Science Laboratory rover. Space Science Reviews, 170(1-4), 583–640. https://doi.org/10.1007/s11214-012-9921-1
- Greeley, R., & Iversen, J. D. (1985). Wind as a geological process: On Earth, Mars, Venus and Titan. Cambridge University Press. Cambridge Planetary Science Series 333.
- Greeley, R., Whelley, P. L., Neakrase, L. D. V., Arvidson, R. E., Bridges, N. T., Cabrol, N. A., et al. (2008). Columbia Hills, Mars: Aeolian features seen from the ground and orbit. *Journal of Geophysical Research*, 113(E6), E06S06. https://doi.org/10.1029/2007JE002971
- Gullikson, A. L., Hayward, R. K., Titus, T. N., Charles, H., Fenton, L. K., Hoover, R., & Putzig, N. E. (2018). Mars global digital dune database (MGD3)—Composition, stability, and thermal inertia (Vol. 2018–1164, p. 17). U.S. Geological Survey Open-File Report. https://doi.org/10. 3133/ofr20181164
- Hamilton, V. E., Christensen, P. R., McSween, H. Y., Jr., & Bandfield, J. L. (2003). Searching for the source regions of Martian meteorites using MGS TES: Integrating Martian meteorites into the global distribution of volcanic materials on Mars. *Meteoritics & Planetary Science*, 38(6), 871–885, https://doi.org/10.1111/j.1945-5100.2003.tb00284.x
- Hanna, R. D., Hamilton, V. E., & Putzig, N. E. (2016). The complex relationship between olivine abundance and thermal inertia on Mars. *Journal of Geophysical Research: Planets*, 121(7), 1293–1320. https://doi.org/10.1002/2015JE004924
- Hayward, R. K., Fenton, L. K., & Titus, T. N. (2014). Mars global digital dune database (MGD3): Global dune distribution and wind pattern observations. *Icarus*, 230(0), 38–46. https://doi.org/10.1016/j.icarus.2013.04.011
- Hayward, R. K., Titus, T. N., Bourke, M. C., Colaprete, A., Christensen, P. R., Mullins, K. F., et al. (2007). Mars global digital dune database and initial science results. *Journal of Geophysical Research E: Planets*, 112(E11). Article Number E11007. https://doi.org/10.1029/2007je002943
- Jakosky, B. M. (1986). On the thermal properties of Martian fines. *Icarus*, 66(1), 117–124. https://doi.org/10.1016/0019-1035(86)90011-4
- Jakosky, B. M., Mellon, M. T., Kieffer, H. H., Christensen, P. R., Varnes, E. S., & Lee, S. W. (2000). The thermal inertia of Mars from the Mars global surveyor thermal emission spectrometer. *Journal of Geophysical Research*, 105(E4), 9643–9652. https://doi.org/10.1029/1999je001088
- Johnson, C., Affolter, M. D., Inkenbrandt, P., & Mosher, C. (2017). An introduction to geology. Salt Lake City Community College. Retrieved from https://opengeology.org/textbook/
- Kieffer, H. H. (2013). Thermal model for analysis of Mars infrared mapping. Journal of Geophysical Research: Planets, 118(3), 451–470. https://doi.org/10.1029/2012JE004164
- Kieffer, H. H., Martin, T. Z., Peterfreund, A. R., Jakosky, B. M., Miner, E. D., & Palluconi, F. D. (1977). Thermal and albedo mapping of Mars during the Viking primary mission. *Journal of Geophysical Research*, 82(28), 4249–4291. https://doi.org/10.1029/js082i028p04249
- Kok, J. F., Parteli, E. J. R., Michaels, T. I., & Karam, D. B. (2012). The physics of wind-blown sand and dust. Reports on Progress in Physics, 75(10), 106901. https://doi.org/10.1088/0034-4885/75/10/106901
- Lancaster, N. (1995). The geomorphology of desert dunes. Routledge.
- Langevin, Y., Poulet, F., Bibring, J. P., & Gondet, B. (2005). Sulfates in the north polar region of Mars detected by OMEGA/Mars express. Science, 307(5715), 1584–1586. https://doi.org/10.1126/science.1109091
- Malin, M. C., & Edgett, K. S. (2001). Mars global surveyor Mars orbiter Camera: Interplanetary cruise through primary mission. *Journal of Geophysical Research*, Planets, 106(E10), 23429–23570. https://doi.org/10.1029/2000je001455
- McEwen, A., Malin, M., Carr, M., & Hartmann, W. K. (1999). Voluminous volcanism on early Mars revealed in Valles Marineris. *Nature*, 397(6720), 584–586. https://doi.org/10.1038/17539
- McKee, E. D. (1979). A study of global sand seas. University Press of the Pacific.
- Mellon, M. T., Fergason, R. L., & Putzig, N. E. (2008). The thermal inertia of the surface of Mars. In J. Bell (Ed.), *The Martian surface: Composition, mineralogy and physical properties* (pp. 399–427). Cambridge University Press.
- Mellon, M. T., Jakosky, B. M., Kieffer, H. H., & Christensen, P. R. (2000). High-resolution thermal inertia mapping from the Mars global surveyor thermal emission spectrometer. *Icarus*, 148(2), 437–455. https://doi.org/10.1006/icar.2000.6503
- Michalski, J., & Bleacher, J. (2013). Supervolcanoes within an ancient volcanic province in Arabia Terra, Mars. Nature, 502(7469), 47–52. https://doi.org/10.1038/nature12482
- Piqueux, S., & Christensen, P. R. (2009). A model of thermal conductivity for planetary soils: 2. Theory for cemented soils. *Journal of Geophysical Research*, 114(E9), E09006. https://doi.org/10.1029/2008JE003309
- Piqueux, S., Kass, D. M., Kleinböhl, A., Slipski, M., Hayne, P. O., McCleese, D. J., et al. (2023). Mars thermal inertia and surface temperatures by the Mars Climate Sounder. *Icarus*, 115851, 115851. https://doi.org/10.1016/j.icarus.2023.115851
- Presley, M. A. (2002). What can thermal inertia do for you? 33rd Lunar and Planetary Science Conference: Houston, Texas. Lunar and Planetary Institute. Abstract #1144.
- Presley, M. A., & Christensen, P. R. (1997a). Thermal conductivity measurements of particulate materials 1. A review. *Journal of Geophysical Research*, 102(E3), 6535–6550. https://doi.org/10.1029/96je03302
- Presley, M. A., & Christensen, P. R. (1997b). Thermal conductivity measurements of particulate materials 2. results. *Journal of Geophysical Research*, 102(E3), 6551–6566. https://doi.org/10.1029/96je03303
- Putzig, N. E., & Mellon, M. T. (2007). Apparent thermal inertia and the surface heterogeneity of Mars. *Icarus*, 191(1), 68–94. https://doi.org/10.1016/j.icarus.2007.05.013
- Putzig, N. E., Mellon, M. T., Herkenhoff, K. E., Phillips, R. J., Davis, B. J., Ewer, K. J., & Bowers, L. M. (2014). Thermal behavior and ice-table depth within the north polar erg of Mars. *Icarus*, 230, 64–76. https://doi.org/10.1016/j.icarus.2013.07.010
- Putzig, N. E., Mellon, M. T., Kretke, K. A., & Arvidson, R. E. (2005). Global thermal inertia and surface properties of Mars from the MGS mapping mission. *Icarus*, 17(2), 325–341. https://doi.org/10.1016/j.icarus.2004.08.017
- Ruff, S. W., & Christensen, P. R. (2002). Bright and dark regions on Mars: Particle size and mineralogical characteristics based on Thermal Emission Spectrometer data. *Journal of Geophysical Research*, 107. https://doi.org/10.1029/2001je001580

BURR ET AL. 16 of 17

- Schorghofer, N., & Edgett, K. S. (2006). Seasonal surface frost at low latitudes on Mars. *Icarus*, 180(2), 321–334. https://doi.org/10.1016/j.icarus. 2005 08 022
- Sébastian, E., Armiens, C., Gomez-Elvira, J., Zorzano, M. P., Martinez-Frias, J., Esteban, B., & Ramos, M. (2010). The rover environmental monitoring station ground temperature sensor: A pyrometer for measuring ground temperature on Mars. Sensors, 10(10), 9211–9231. https:// doi.org/10.3390/s101009211
- Silvestro, S., Fenton, L. K., Vaz, D. A., Bridges, N. T., & Ori, G. G. (2010). Ripple migration and dune activity on Mars: Evidence for dynamic wind processes. *Geophysical Research Letters*, 37(20), L20203. https://doi.org/10.1029/2010gl044743
- Silvestro, S., Vaz, D. A., Ewing, R. C., Rossi, A. P., Fenton, L. K., Michaels, T. I., et al. (2013). Pervasive aeolian activity along rover Curiosity's traverse in Gale Crater, Mars. *Geology*, 41(4), 483–486. https://doi.org/10.1130/g34162.1
- Silvestro, S., Vaz, D. A., Fenton, L. K., & Geissler, P. E. (2011). Active aeolian processes on Mars: A regional study in Arabia and Meridiani Terrae. *Geophysical Research Letters*, 38(20), L20201. https://doi.org/10.1029/2011gl048955
- Tirsch, D., Jaumann, R., Pacifici, A., & Poulet, F. (2011). Dark aeolian sediments in Martian craters: Composition and sources. *Journal of Geophysical Research*, 116(E3), E03002. https://doi.org/10.1029/2009je003562
- Urso, A., Chojnacki, M., & Vaz, D. A. (2018). Dune-Yardang interactions in becquerel crater, Mars. *Journal of Geophysical Research: Planets*, 123(2), 353–368. https://doi.org/10.1002/2017JE005465
- Whelley, P., Matiella Novak, A., Richardson, J., Bleacher, J., Mach, K., & Smith, R. N. (2021). Stratigraphic evidence for early martian explosive volcanism in Arabia Terra. *Geophysical Research Letters*, 48(15). https://doi.org/10.1029/2021GL094109e2021GL094109

BURR ET AL. 17 of 17